



1 **A particle based model for soil water dynamics: how** 2 **to match and step beyond Richards' equation?**

3 Erwin Zehe¹ and Conrad Jackisch¹

4 1) Karlsruhe Institute of Technology (KIT)

5 Abstract:

6 Within this study we propose a stochastic approach to simulate soil water dynamics in the
7 unsaturated zone by using a non-linear, space domain random walk of water particles. Soil
8 water is represented by particles of constant mass, which travel according to the Itô form of
9 the Fokker Planck equation. The model concept builds on established soil physics by
10 estimating the drift velocity and the diffusion term based on the soil water characteristics. A
11 naive random walk, which assumes all water particles to move at the same drift velocity and
12 diffusivity, overestimated depletion of soil moisture gradients compared to a Richards' solver.
13 This is because soil water and hence the corresponding water particles in smaller pore size
14 fractions, are, due to the non-linear decrease of soil hydraulic conductivity with decreasing
15 soil moisture, much less mobile. After accounting for this subscale variability of particle
16 mobility, the particle model and a Richards' solver performed similarly during simulated
17 wetting and drying circles in three distinctly different soils. The particle model typically
18 produced slightly smaller top soil water contents during wetting and was faster in depleting
19 soil moisture gradients during subsequent drainage phases. Within a real world benchmark the
20 particle model matched observed soil moisture response to a moderated rainfall event even
21 slightly better than the Richards' solver. The proposed approach is hence a promising, easy to
22 implement alternative to the Richards equation. This is particularly also because it allows one
23 to step beyond the assumption of local equilibrium during rainfall driven conditions. This is
24 demonstrated by treating infiltrating event water particles as different type of particle which
25 travel initially, mainly gravity driven, in the largest pore fraction at maximum velocity, and
26 yet experience a slow diffusive mixing with the pre-event water particles within a
27 characteristic mixing time.

28 Key words: soil water dynamics, random walk, Lagrange model, pre-event water, mobile and
29 immobile water



30 1 INTRODUCTION

31 Only a tiny amount of water is stored in the unsaturated zone: with an estimated volume of
32 about 16,500 km³ (Dingman, 1994), soil moisture represents 0.05% of total fresh water.
33 Nevertheless, this tiny storage amount exerts first order control on the partitioning of net
34 radiation energy in latent and sensible heat flux (Kleidon and Renner, 2013a, b; Gayler et al.,
35 2014; Turner et al., 2014) - maybe the key process in land surface atmosphere exchange.
36 Crucially, soil moisture crucially controls CO₂ emissions of forest soils (Koehler et al., 2010),
37 de-nitrification and related trace gas emissions into the atmosphere (Koehler et al., 2012) as
38 well as metabolic transformations of pesticides (e.g. Holden and Fierer, 2005).
39 Notwithstanding soil moisture controls splitting of rainfall into surface runoff and
40 (preferential) infiltration (Zehe et al., 2007; Loos and Elsenbeer, 2011; Graeff et al., 2012;
41 Zimmermann et al., 2013; Bronstert et al., 2012; Klaus et al., 2014). Soil water is furthermore
42 a key factor limiting vegetation dynamics in savannah ecosystems (Saco et al., 2007; Tietjen
43 et al., 2010).

44

45 Water storage in the unsaturated zone is controlled by capillary forces which increase
46 nonlinearly with decreasing pore size, because water acts as a wetting fluid in soil (Horton
47 and Jury, 2004). The standard approach to represent capillary and gravity controlled soil water
48 dynamics is the Darcy-Richards equation in combination with suitable soil water
49 characteristics. This continuum model essentially assumes that capillarity controlled diffusive
50 fluxes dominate soil water dynamics under local equilibrium conditions even during rainfall
51 driven conditions. Today we know that the assumptions of local equilibrium conditions e.g.
52 (Hassanizadeh et al., 2002; Neuweiler et al., 2012) and a mainly diffusive flow are often not
53 appropriate, particularly during rainfall events in structured soils. Rapid or preferential flow
54 imply a strong local disequilibrium and imperfect mixing between a fast fraction of soil water,
55 travelling in interconnected coarse pores or non-capillary macropores (Šimůnek et al., 2003;
56 Klaus et al., 2013), and the slower diffusive flow in finer fractions of the pore space. As
57 outlined in a couple of excellent review articles (e.g. Šimůnek et al., 2003; Beven and
58 Germann, 2013), up to now many concepts have been proposed to overcome the inability of
59 the Darcy – Richards concept to cope with not-well mixed or even non capillary, preferential
60 flow. These concepts range from a) early stochastic convection (Jury, 1982), b) dual porosity
61 and permeability approaches assuming overlapping and exchanging continua (Gerke and van
62 Genuchten, 1993; van Schaik et al., 2014), to c) spatially explicit representation of



63 macropores as vertically and laterally connected flow paths (Vogel, 2006; Klaus and Zehe,
64 2010; Zehe et al., 2010a; Wienhoefer and Zehe, 2014) and d) non local formulations of the
65 Richards equation (Neuweiler et al., 2012). Notwithstanding the listed shortcomings, the
66 Darcy Richards concept works well when soil water dynamics are dominated by capillarity
67 particularly during radiation driven conditions (Zehe et al., 2010b; Zehe et al., 2014).
68 Furthermore, it would be foolish to mistake the limitations of the Richards equation with non-
69 importance of capillary forces in soil. Without capillarity infiltrating rainfall would drain into
70 groundwater bodies, leaving an empty soil as the local equilibrium state - there would be no
71 soil water dynamics at all, probably even no terrestrial vegetation and the water cycle would
72 operate in a complete different manner without capillary forces. Better alternatives for the
73 Darcy-Richards approach are thus highly desirable, as long they preserve the grain of “truth”
74 about capillarity as underlying key control.

75

76 Here we propose such an alternative approach to simulate soil moisture dynamics in an
77 effective, stochastic and yet physical way. Specifically, we hypothesise that soil water flow
78 can be simulated by means of non-linear random walk, representing soil water by a variable
79 number of particles. To the best of our knowledge, similar Lagrangian approaches were
80 proposed by Davies and Beven (2012) and taken much further by Ewen (1996b, a). In
81 accordance with the latter approach our model concept is essentially built on capillarity by
82 making use of soil physics and established soil water characteristics. Particle tracking based
83 on a random walk is usually employed for simulating advective-dispersive transport of solutes
84 in the water phase, but not for the soil water phase itself (Delay and Bodin, 2001; Klaus and
85 Zehe, 2011; Dentz et al., 2012). For linear problems, when neither the dispersion coefficient
86 nor the drift term depend on solute concentration and thus particle density, a time domain
87 representation of the random walk is favourable as it maximises computational efficiency
88 (Dentz et al., 2012). Non-linear problems, such as transport of nonlinearly adsorbing solutes
89 or the envisaged simulation of soil water dynamics, require a space domain, random walk,
90 because the drift and diffusion term change non-linearly with changing particle density. An
91 integral treatment is, hence, inappropriate as the superposition principle is invalid for non-
92 linear problems.

93

94 In the following we introduce the model concept and present different benchmarks to test its
95 capability to simulate soil moisture dynamics during equilibrium and non-equilibrium



96 conditions. More specifically we a) detail the underlying theory and model implementation, b)
 97 reflect on obvious and non-obvious implications of treating water flow in a porous medium as
 98 a non-linear random walk and c) propose a straight forward way to treat non equilibrium
 99 infiltration in section 2. Section 3 explains the model benchmarking a) against a model based
 100 on the Darcy-Richards concept for various soils, initial and boundary conditions as well as b)
 101 against soil moisture observations obtained in the Weiherbach catchment in Germany. After
 102 presenting the results in section 4, we close with discussion and conclusions in section 5.

103 2 THEORY AND MODEL IMPLEMENTATION

104 2.1 A random walk approach for diffusive water flow in the soil matrix

105 Our starting point is the equivalence of the Richards equation in the soil moisture based form
 106 to the advection dispersion equation (Jury and Horton, 2004):

$$107 \quad \frac{\partial \theta}{\partial t} = -k(\theta) + \frac{\partial}{\partial z} \left(D(\theta) \frac{\partial \theta}{\partial z} \right) \quad (\text{Eq.1})$$

$$D(\theta) = k(\theta) \frac{\partial \psi}{\partial \theta}$$

108 The volumetric soil water content $\theta [\text{L}^3/\text{L}^3]$ corresponds to the concentration $C [\text{M}/\text{L}^3]$ in the
 109 advection diffusion equation; the first term corresponds to a trivial drift/advection term
 110 $u(\theta) = k(\theta) [\text{L}/\text{T}]$ characterizing downward advective water fluxes driven by gravity. The
 111 second term corresponds to the dispersive/diffusive solute flux, by representing diffusive
 112 water movements driven by the soil moisture gradient and controlled by the diffusivity $D(\theta)$
 113 $[\text{L}^2/\text{T}]$ of soil water. D is the product of the hydraulic conductivity $k(\theta)$ and the slope of the
 114 soil water retention curve $\frac{\partial \psi}{\partial \theta}$. This equivalence and the work of Ewen (1996 a, b) motivated
 115 the idea to simulate soil water movement by a random walk of a large number of particles.
 116 The soil moisture profile at a given time and within a given spatial discretisation is
 117 represented by the spatial density of “water particles” at this time. Water particles are constant
 118 in mass and volume. The trajectory of a single particle within a time step Δt is described by
 119 the Itô form of the Fokker Planck equation:

$$120 \quad z(t + \Delta t) = - \left(k(\theta(t)) + \frac{\partial D(\theta(t))}{\partial z} \right) \cdot dt + Z \sqrt{6 \cdot D(\theta(t)) \cdot \Delta t} \quad (\text{Eq. 2})$$



121 With Z being a random number, uniformly distributed between $[1,-1]$, (note when using
122 random numbers from the standard normal distribution the drift term is $\sqrt{2 \cdot D(\theta(t)) \cdot \Delta t}$). The
123 term $\frac{\partial D(\theta)}{\partial z}$ corrects the drift term in the case of a spatial variable diffusion as
124 recommended by (Kitanidis, 1994; Roth and Hammel, 1996; Michalak and Kitanidis, 2000;
125 Elfeki et al., 2007; Uffink et al., 2012). The main difference to the usual linear random walk is
126 that D and k depend on soil moisture and thus the water particle density. Here we
127 parameterise this dependence by means of the van-Genuchten (1980) and Mualem (1976)
128 model (Figure 1).

129 **2.2 Challenges of the particle based approach**

130 **2.2.1 Non-linear dependence of D and k on particle density**

131 The obvious implication of the non- linear dependence of the drift velocity and diffusion term
132 on the soil water content is that a short time stepping in combination with at least a predictor
133 corrector scheme is needed to account for the non-linear change of both parameters during an
134 integration time step.

135

136 The non-obvious implication arises from the fact that the soil water retention curve reflects
137 the cumulative pore size distribution of the soil (Jury and Horton, 2004) and the actual soil
138 moisture reflects water that is stored among different size fractions of the wetted pore space.
139 It is well known that water flow velocity decreases with decreasing pore size, which is
140 reflected in the non-linear decrease in soil hydraulic conductivity with decreasing soil water
141 content. However, this non-linear decrease implies that the water particles representing the
142 actual soil water content $\theta(t)$ do not all travel at the same constant drift velocity $k(\theta(t))$ and
143 diffusivity $D(\theta(t))$. In fact only a small fraction of the particles, representing the water in the
144 largest wetted pores, travels according to these values; the remaining water particles,
145 representing water stored in smaller pores, are much less mobile.

146

147 Hence, the $D(\theta(t))$ and $k(\theta(t))$ curves between the actual soil water content (Figure 1) and
148 their minimum values may be regarded as a distribution function of the random walk
149 parameters among the water particles that represent a given soil water content. Essentially, we
150 propose that a correct random walk implementation needs to account for the different mobility
151 of the water particles in different pore sizes by resampling the D and k curves from their
152 minimum to the actual values with a suitable numbers of bins. Contrarily, we expect a naive



153 execution of Eq. (2), assuming that all particles in a given grid element as equally mobile
154 according to $k(\theta(t))$ and $D(\theta(t))$, to overestimate fluxes and depletion soil moisture gradients.

155 **2.2.2 The necessity to operate at high particle numbers**

156 Another challenge when treating water flow in a Lagrangian approach is that a much larger
157 number of particles is necessary compared to random walk applications of solute transport.
158 Why so? The latter treats cases when a solute invades a domain with a small or zero
159 background concentration of this solute. The total solute mass in the system can thus be
160 represented by the order of $10^4 - 10^5$ particles even in large, two-dimensional domains at a
161 good signal-to-noise ratio (Roth and Hammel, 1996; Zehe et al., 2001). In the case of soil
162 water dynamics the “background concentration”, i.e. the stored pre-event water mass in the
163 soil profile, is much larger than the input signal of infiltrating event water. The particle
164 number must thus be considerably increased to the order of 10^6 in a one dimensional domain,
165 to ensure that the rainfall input is represented by a number of particles which is sufficiently
166 high for a stochastic approach.

167 **2.3 Equilibrium and non-equilibrium infiltration**

168 Infiltration into the soil at a given $\theta(t)$ is represented as input of event water particles $N^{\text{in}}(t)$
169 into the upper model element, thereby changing the soil water content by $\Delta\theta$. Local
170 equilibrium conditions, as assumed in the Darcy-Richards concept, imply that water infiltrates
171 into the smallest non-wetted part of the pore space (as sketched in Figure 1). Consequently the
172 random walk of the event and pre-event water particles in the largest wetted pores is
173 determined by $D(\theta(t)+\Delta\theta)$ and $k(\theta(t)+\Delta\theta)$ (Figure 1).

174
175 A straightforward approach to account for non-equilibrium infiltration is to assume that event
176 water enters into and travels in the coarsest pores of the soil, thereby wetting the path of
177 minimum flow resistance. This implies that diffusive mixing from these coarse pores into the
178 smallest non-wetted part of the pore space is much slower than the gravity driven downward
179 flow. Non-equilibrium infiltration may hence be simulated, by assigning the saturated
180 hydraulic conductivity k_s as drift term “event water particles” and assuming small diffusive
181 mixing, for instance the lower 5 or 10% quantile of $D(\theta)$. From the latter we specify the time
182 scales for the event water to mix with the pre-event water as explained further in section 3.2.



183 **2.4 Model implementation and execution**

184 **2.4.1 Model parameters, initial and boundary conditions**

185 The proposed water particle model is coded in Matlab and requires in its simplest form the
186 same parameters, initial and boundary conditions as a numerical solver of the Richards
187 equation (soil hydraulic functions for the entire soil profile as well as rainfall and optionally
188 evaporation time series). Although the random walk itself does not require a spatial
189 discretisation, we employ a grid to calculate particle densities and soil water contents during
190 run time. The model can be initialized using either an initial soil moisture or matric potential
191 profile for the selected spatial discretisation and based on the selected initial number of water
192 particles N^{ini} . The particle mass m [M] is equal to the integral water mass of the initial state
193 divided by N .

194

195 Initial positions of the pre-event water particles in a given grid cell are uniformly distributed.
196 Infiltration or soil evaporation is represented as particle input $N^{\text{in}}(t)$ or loss $N^{\text{out}}(t)$ into/from
197 the upper model element, by dividing the infiltrated/evaporated water mass in a time step by
198 the particle mass. Infiltrating particles start at $z=0$. Depending on the selected lower boundary
199 condition, particles may either freely drain from the domain (free drainage boundary), a fixed
200 number of particles is kept (constant head boundary), or particles are not allowed to leave the
201 domain (zero flux boundary).

202

203 For the implementing non-equilibrium infiltration we treat event water particles as separate
204 type of particles (Figure 1), similar to a different kind of solute that is not influenced by the
205 pre-event water particles unless both fractions are well mixed. Shortly after infiltration we
206 assume event particles to be mainly controlled by gravity; they travel into the vertical
207 according to $k(\theta_s)$ and experience a small diffusive motion characterized by D_{mix} . D_{mix}
208 determines the time scale at which pre-event and event water particles get mixed (compare
209 Eq. 3) Non equilibrium implies that the time scale for diffusive mixing t_{mix} is much larger
210 than the time scale of advective transport through a grid element Δz t_{ad} , which implies the grid
211 Peclet number being much larger than 1:

212



$$\frac{\Delta z k_s}{D_{mix} t_{ad}} = \frac{t_{mix}}{t_{ad}} \gg 1$$

$$t_{mix} = \frac{(\Delta z)^2}{D_{mix}}; t_{ad} = \frac{\Delta z}{k_s} \quad (\text{Eq. 3}).$$

214

215 Based on this time scale mixing can be characterised by, for instance, using an exponential
 216 distribution (as proposed by Davies and Beven, 2012). In our study we selected an even
 217 simpler approach, assuming uniformly distributed mixing between the time when the particle
 218 enter the domain and the mixing time. This approach maximises the entropy of the mixing
 219 process (Klaus et al., 2015) thereby minimizing the number of a-priory assumption; because
 220 mixing of each particle is equally likely..

221

222 2.4.2 Time stepping and subscale variability of particle mobility

223 For model execution we choose a predictor corrector scheme: we predict the particle
 224 displacement for $0.5 \cdot \Delta t$, based on $k(\theta(t))$, $D(\theta(t))$, update $\theta(t+0.5 \cdot \Delta t)$ based on the new
 225 particle density distribution and compute the full time step using $k(\theta(t+0.5 \cdot \Delta t))$,
 226 $D(\theta(t+0.5 \cdot \Delta t))$. As $k(\theta(t))$ and $D(\theta(t))$ are only available at the discrete nodes of the
 227 simulation grid, these are interpolated to the particle locations using inverse distance weights.

228

229 We tested two different approaches to cope with the above explained non-linear dependence
 230 of D and k on $\theta(t)$ and thus on particle density. The first, referred to as “full mobility mode”,
 231 distributes D among the particles to resemble the shape of D between $D(\theta_r)$ and $D(\theta(t))$ and of
 232 k between $k(\theta_r)$ to $k(\theta(t))$ (Figure 1). To this end we subdivided the particles in a grid cell
 233 representing the actual soil water content $\theta(t)$ and the D and k curves in 800 bins (Figure 1).
 234 This full mobility approach does, however, imply the need to calculate a large chunk of rather
 235 marginal displacements as k and D decline rather fast. The computational less extensive
 236 alternative is to calculate the displacement according to Eq. 2 exclusively for the fastest 10 or
 237 20 % of water particles and assuming the remaining ones to be immobile. Of key interest in
 238 this context is also the question whether the fast mobile and the slow immobile particles
 239 fractions mix across the pores size fractions or not (Brooks et al., 2010). Mixing can be
 240 implemented by assigning the particles randomly to the different bins of during each time step
 241 $D(\theta)$, while no mixing can be realised by always assigning the same particle to same pore size



242 fraction/ “mobility class”. Within our simulations we tested both options. The second option
243 turned out to be clearly superior with respect to matching simulations with a Richards’ solver.

244 **3 MODEL BENCHMARKING**

245 **3.1 Particle model versus Richards equation**

246 In a set of benchmarks we compared the particle model to a numerical solver of the Richards
247 equation, which was also implemented using Matlab using the same predictor corrector
248 scheme. We simulated wetting and drying cycles for three soils with rather different soil water
249 characteristics (Table 1). The first is a sandy soil developed on limestone located in the Attert
250 experimental basin in Luxembourg (Martinez-Carreras et al., 2010; Wrede et al., 2015). The
251 second is a young highly porous and highly permeable soil on schistose periglacial deposits in
252 the Attert basin, which predominantly consists of fine silt aggregates with relative coarse
253 inter-aggregate pores. The third is a Calcaric Regosol on loess with a large fraction of
254 medium size pores, which is located at the central meteorological station in the Weiherbach
255 catchment in south western Germany.

256

257 These soils were exposed to simulated wetting and drying cycles characterized in Table 2, by
258 combining block rains of different intensity with periods of no flux at the upper boundary.
259 Thereby we compared two different initial soil moisture profiles: a uniform soil water content
260 of $0.269 \text{ m}^3 \text{ m}^{-3}$ and an s-shaped profile. The intensities of block rain events were selected to
261 be small enough to avoid infiltration excess. Feasible time steps to avoid noisy soil moisture
262 profiles vary between 60 s for the sand and the young soil on schist and 200 s for the Calcaric
263 Regosol, when using an initial number of particles of $N^{\text{ini}} = 6 * 10^5$. Both models operated at a
264 constant grid size of 0.05 m in a model domain with a vertical extent of 1.5 m.

265 **3.2 Real world benchmark: moderate rainfall event on a loess soil**

266 In the second benchmark we evaluated the particle model against moisture dynamics observed
267 at the central meteorological station in the Weiherbach catchment (Zehe et al., 2001; Plate and
268 Zehe, 2008). At this site past rainfall records and soil moisture records in 0.025, 0.1, 0.2, 0.3
269 and 0.4m are available at a 10 min resolution. We carefully selected a moderate nocturnal
270 rainfall event, to avoid the influence of macropore flow and evaporation on wetting and
271 subsequent drying. The event had a total depth of 4 mm with maximum rainfall intensity of 2
272 mm/h, started at the 9th of May at 1:15 and lasted until 4:15 a.m. The changes in soil moisture



273 in the upper layers revealed a recovery of 90% of the rainfall water, which implies that a
274 small fraction of the water might have bypassed the sensors.

275

276 Both models were operated at a finer spatial discretisation of 0.025 m and we set the number
277 of pre-event particles to $1 \cdot 10^6$. The simulation period ranged from 0:05 until 5:45 a.m. at this
278 day, to allow for a drainage period but to stop simulation before evaporation in the natural
279 system kicked in. Hydraulic properties of the top and subsoil of the Calcaric Regosol are
280 given in Table 3. Both models were initialised by assigning the observed soil moisture values,
281 which increased from $0.18 \text{ m}^3 \text{ m}^{-3}$ in 0.025 m to $0.33 \text{ m}^3 \text{ m}^{-3}$ in 0.4 m depths, using inverse
282 distance interpolation between the grid nodes. As no surface runoff occurred during this
283 event, rainfall was treated as a flux boundary condition.

284 4 RESULTS

285 In the following we present final soil moisture profiles simulated with the Darcy - Richards
286 and the particle model for selected runs and compare the temporal evolution of soil moisture
287 profiles in form of 2d colour plots. In terms of computing time we noted no remarkable
288 difference between the particle model and the Richards solver. This is because the code is
289 implemented by relying almost exclusively on array operations, thereby avoiding time-
290 consuming loops over all particles.

291 4.1 Particle model versus Richards equation

292 4.1.1 Sandy soil on lime stone

293 Figure 2 presents the final soil moisture profiles for both models for selected simulation
294 experiments. Panel a) reveals that a treatment of soil moisture dynamics as naïve random
295 walk, when all particles travel according to $D(\theta(t))$ and $k(\theta(t))$, implies clearly - as expected -
296 - too fast mixing of event water particles into larger depths compared to the Richards
297 equation. However, when we accounted for the different mobility of water particles in
298 different pore sizes, by resembling the distribution of D and k between $D(\theta_r)$ to $D(\theta(t))$ and
299 $k(\theta_r)$ to $k(\theta(t))$, the particle model closely matched the soil moisture dynamics simulated with
300 the Richards equation for all simulated wetting cycles. This can be deduced from panels b)
301 and c) in Figure 2, which show the simulated soil moisture profiles which evolved from a
302 uniform initial state after a block rain input of 20 and 40 mm, respectively. Panel d) in Figure
303 2 additionally corroborates the highly similar performance of both models when starting from



304 the s-shaped initial state. For the sandy soil also we found in general a very good agreement
305 between the “full mobility” particle model and a simulation assuming a mobile fraction of
306 20% (solid green line Figure 2 b).

307

308 Figure 3 presents the temporal evolution of simulated soil moisture profiles in the form of 2d
309 colour plots during a 1h block rain of 40 mm (panels a and c) and during a 1h block rain of 20
310 mm and subsequent drainage of 3h (panels c and d). The accordance between the Richards
311 solver and the full mobile particle model during rainfall driven conditions was generally high,
312 regardless of the initial states and rainfall intensities. Small differences occurred in the case of
313 the 40 mm rainfall, where the particle model produced a slightly larger soil moisture at the
314 end of the wetting period (Figure 3 panels a) and c)). During non-driven conditions the
315 particle model was generally faster in depleting soil moisture gradients compared to the
316 Richards model, as depicted in panels b) and d) in Figure 3.

317 **4.1.2 Young silty soil on schist**

318 Simulations of soil water dynamics for the young silty soil on schist, revealed clearer
319 differences between the Richards equation and the full mobility particle model. The final soil
320 moisture profiles simulated with the particle model showed smaller values in the upper 20 cm
321 but larger values between 20 and 40 cm as the corresponding profiles simulated with the
322 Richards solver (Figure 4, all panels). Differences between simulations of the particle model
323 operated in the full mobility mode and at a mobile fraction of 20% (Figure 4 panel a) were as
324 small as in the sandy soil. A better match of the Richards solver required a reduction in the
325 mobile particle fraction to 10 % (solid green line in panel Figure 4 a). This different behaviour
326 is likely explained by the larger fraction of medium and small pores in the silty soil compared
327 to the sandy soil. When simulating a stronger rainfall forcing of 40 mm for 1h both the
328 Richards’ solver and the full mobility particle model were in slightly better accordance as in
329 the case of the 20 mm input (Figure 4 panel b), while the systematic deviations remained
330 similar.

331

332 The particle model was also more efficient in this soil in depleting sharp soil moisture
333 contrasts, which became particularly visible when starting with the s-shaped initial soil
334 moisture profile (Figure 4, panel c). The stronger dissipative character of the particle model
335 manifested itself even clearer during subsequent drainage periods following on from
336 infiltration events. This is shown for the case of 20 mm infiltration of the uniform initial state



337 and subsequent 2 h drainage in the form of 2d colour plots in Figure 5 and for the
338 corresponding final state in Figure 4 d).

339 **4.1.3 Calcaric Regosol on loess**

340 Simulations of soil water dynamics for the Calcaric Regosol on loess were pretty consistent
341 with those carried out for the young silty soil on schist, particularly with respect to the
342 systematic differences between the Richards and the particle model. For a total infiltration of
343 15 mm in 3 h the top 10 to 20 cm, soil moisture simulated with the Richards model was
344 slightly larger than soil moisture simulated with the full mobility particle model, between 10
345 to 40 cm it was the other way around (Figure 6 a and b). Again we achieved a better match of
346 the Richards model when operating the particle model at a mobile fraction of 10%. In general,
347 differences in model behaviour were more distinct than in the in case of the silty soil on
348 schist. This is likely explained by the even finer pore sizes in the Calcaric Regosol, which is
349 reflected in the corresponding air entry values in Table 1.

350

351 The finer pore sizes and wider pore size distribution explain also the even stronger dissipative
352 characters of the full mobility particle model during drainage periods, as corroborated by the
353 response starting either with the uniform or the s-shaped initial state to 15 mm infiltration in 3
354 h and 9 h subsequent drainage (Figure 6 c and d). The particle model is faster in redistributing
355 the water from between the top and the subsoil, which implies smaller soil moisture values
356 compared to the Richards solver in the upper 0.30 m, but larger soil moisture values between
357 0.3 and 0.5 m.

358 **4.2 Real world benchmark**

359 The real world benchmark in the Calcaric Regosol revealed that the particle model operated in
360 the full mobility mode performed differently - but not necessarily worse – when compared to
361 the Richards solver. This can be deduced from the comparison of simulated soil moisture
362 profiles to observations at the end of the rainfall event (Figure 7 a) and at the end of the
363 simulation (Figure 7 b). Both models overestimated wetting in 0.025 m, while the particle
364 model was slightly closer to the observed values at both time steps. The observed wetting of
365 $0.02 \text{ m}^3 \text{ m}^{-3}$ in 10 cm at the end of the simulation was well matched by the particle model but
366 underestimated by the Richards-solver.

367

368 A possible explanation for the overestimation of the soil moisture change in 0.025 m by the
369 models, which is consistent with a non-closed water balance, is that a part of the rainfall water



370 bypassed the measurement device due fast non-equilibrium infiltration in connected coarse
371 pores. To test this idea, we performed additional simulations by treating infiltrating event
372 water particles as a second particle type infiltrating into the largest pores, which uniformly
373 mixed with the pre-event water particles within the time t_{mix} . Figure 7 c) and d) compare the
374 event water content and total content (as the sum of pre-event and mixed water) for two
375 different mixing times $t_{\text{mix}} = 4004$ ($D_{\text{mix}} = 1.5 \cdot 10^{-7} \text{ m}^2\text{s}^{-1}$) and 17144 ($D_{\text{mix}} = 3.3 \cdot 10^{-8} \text{ m}^2\text{s}^{-1}$),
376 which correspond the lower 50 or 30 % quantiles of $D(\theta)$, respectively. Particularly, the model
377 with the longer mixing time performed distinctly differently to the particle model, assuming
378 well mixed infiltration. Event water infiltrates and bypasses the pre-event water to a depth of
379 between 0.1 and 0.3 m in a clearly advective fashion. Related volumetric pre-event water
380 contents peak at $0.04 \text{ m}^3\text{m}^{-3}$ (Figure 7 c and d). Consequently, the rainfall input leaves a much
381 weaker signal in the well mixed water fraction (Figure 8 c), reflecting those event water
382 particles which diffusively travelled from the coarse pore fraction into the smallest non-
383 wetted fraction. In case of the faster mixing most of the event water is already mixed with the
384 pre-event water at the end of the rainfall event (Figure 7 c) and water is completed mixed at
385 the end of the simulation (Figure 7 d). Consequently, the differences with the simulation
386 assuming equilibrium infiltration are much less pronounced.

387

388 None of the selected mixing time scales did however yield a systematic better performance of
389 the particle model, in a sense that the mixed water fraction, which we assumed to be in good
390 contact with the TDR, better matched the observation at 0.025 m depth. This is corroborated
391 for the final states in Figure 8 c) and d). We thus performed an additional model run assuming
392 a diffusive mixing according to the 40 % quantile of $D(\theta)$, which corresponds to $t_{\text{mix}} = 7800$ s
393 ($D_{\text{mix}} = 8.8 \cdot 10^{-8} \text{ m}^2\text{s}^{-1}$). In this case the simulated well mixed water content was at both times
394 and in good accordance with the observations at 0.025 m and 0.1 m. We may, hence, state that
395 the proposed explanation is feasible and that the particle model allows treatment of non-
396 equilibrium infiltration in a straightforward manner.

397 5 DISCUSSION AND CONCLUSIONS

398 5.1 Subscale variability of water particles – the key to a reasonable 399 performance of non-linear random walk

400 This study provides evidence that a non-linear, random walk of water particles is a feasible
401 alternative to the Richards equation for simulating soil moisture dynamics in the unsaturated



402 zone. The model preserves capillarity as first order control and estimates the drift velocity and
403 the diffusivity term based on the unsaturated soil hydraulic conductivity and the slope of the
404 soil water retention curve. As expected, a naive random walk, when all particles in a grid
405 element travel according to $k(\theta(t))$, $D(\theta(t))$, overestimated depletion of soil moisture gradients
406 compared to the Richards solver within three different soils for all tested initial and boundary
407 conditions. The key for improving the particle model performance was to account for the fact
408 that soil water in different pore size fractions is not equally mobile. When accounting for this
409 subscale variability in particle mobility in different pore sizes by resampling the D and k
410 curves from their minimum to the actual values with a suitable numbers of bins, the particle
411 model performed in good accordance with but yet differently to a Richards solver in three
412 distinctly different soils. Both models generally gave better accordance during rainfall driven
413 conditions, regardless of the intensity of the rainfall forcing and the shape of the initial state;
414 except that the particle model produced slightly smaller top soil water contents. Within
415 subsequent drying cycles the particle was typically faster in depleting soil moisture gradients
416 than the Richards' model. This general pattern became more distinct than for a sandy soil
417 when running models in a finer porous soil consisting of silty aggregates and in a Calcific
418 Regosol on loess.

419 **5.2 Learning about inherent assumption and stepping beyond limitations of** 420 **the Richards approach**

421 Alternatively, we tested a less computational demanding approach, assuming only the 10 or
422 20% of the fasted particles to be mobile, while treating the remaining particles located in
423 smaller pores sizes as immobile. In the case of the sandy soil a mobile fraction of 20%
424 revealed almost identical results as the full mobility model and performed even closer to the
425 Richards solver. In the two closer soils the mobile fraction mode was generally less dispersive
426 than the full mobility model and again in better accordance with the Richards solver,
427 particularly when setting the mobile particle fraction to 10%. In this context we compared
428 also the cases of perfect mixing and no mixing between mobile and immobile water particles
429 between different time steps (as explained in section 2.4.2). The second option was clearly
430 superior with respect to matching simulations with a Richards' solver, while the other yielded
431 strong differences. We may thus state that the particle model is a suitable tool to “unmask” a)
432 inherent implications of the Darcy-Richards concept on the fraction of soil water that actually
433 contributes to soil water dynamics and b) the inherent very limited degrees of freedom for
434 mixing between mobile and immobile water fractions. Our findings suggest, furthermore, that



435 the idea of two separate water worlds, one supplying runoff the other supplying transpiration,
436 which is advocated in Brooks et al. (2010), is a somewhat naïve interpretation of soil physics
437 and the inherently low degrees of freedom water to mix across pores size fractions, than a real
438 mystery.

439

440 In a real world benchmark the particle model matched observed soil moisture reactions in
441 response to a moderate rainfall event even better than the Richards solver. However, both
442 models clearly overestimated top soil wetting compared to observations. An asset of the
443 particle based approach is that the assumption of local equilibrium equation during infiltration
444 may be easily ignored. Specifically we did this to test the idea whether bypassing of a fast
445 water fraction might explain the model bias in the topsoil. To this end infiltrating event water
446 particles were treated as second particle type, which travel initially mainly gravity driven in
447 the largest pore fraction at maximum drift, and yet experience a slow diffusive mixing with
448 the pre-event water particles within a characteristic mixing time. Simulations with the particle
449 model in the non-equilibrium mode performed evidently distinctly different in the topsoil, and
450 were rather sensitive to the diffusion coefficient D_{mix} describing mixing of event water
451 particles. When assuming D_{mix} equal to the 40% quantile of the D -(θ) curve, the mixed water
452 fraction of the particle model was in good accordance with observed soil moisture changes
453 at 0.025 and 0.1 m depths after the rainfall and at the end of the simulation period.

454

455 Our findings are in line with the early findings of Ewen (1996b). The diffusive mixing term
456 parameter D_{mix} is perhaps easier to interpret as the λ parameter Ewen (1996b) introduced to
457 account for displacement of old water by new water particles, notwithstanding that
458 displacement of pre-event water seems to play a key role in feeding macropore flow (Klaus et
459 al, 2013; Klaus et al., 2014). Contrary to the exponential mixing term Davis and Beven (2012)
460 introduced to stop rapid flow in the MIP model, we used a uniform distribution which
461 maximizes entropy of the mixed particles (Klaus et al., 2015).

462 **5.3 Conclusions and Outlook**

463 We conclude overall that the proposed non-linear random walk of water particles is an
464 interesting stochastic alternative for simulating soil moisture dynamics in the unsaturated
465 zone, which preserves the influence of capillarity and makes use of established soil physics.
466 The approach is easy to implement, even in two or three dimensions and fully mass
467 conservative. The drawback is the required high density of particles, arising from the small



468 ratio of event water to pre-event water in soil, which might become a challenge when working
469 in larger domains and several dimensions. However, due to its simplicity the model is straight
470 forward to implement on a parallel computer.

471

472 The particle approach is particular interesting, as the implementation of fast non-equilibrium
473 infiltration and the separation of event and pre-event water is straight forward, compared to
474 for instance a non-local formulation of the Richards equation (Neuweiler et al., 2012). In line
475 with Ewen (1996) we hence regard particle based models as particularly promising to deal
476 with preferential transport of solutes (optionally also heat), and to explore transit time
477 distributions in a forward mode.

478

479 We are aware, that the evidence we provided here is a somewhat tentative first step
480 corroborate the flexibility of the particle based approach to include non-equilibrium flow and
481 matrix flow in the same stochastic, physical framework. A much more exhaustive treatment of
482 this issue is provided in a forthcoming study which presents and extension of the concept to a
483 2 dimensional domain with topologically explicit macropores and the test of concurring
484 hypothesis to represent infiltration into macropores as well as macropore matrix interactions.

485

486 ACKNOWLEDGMENTS

487 This study contributes to and greatly benefited from the "Catchments As Organized Systems"
488 (CAOS) research unit. We sincerely thank the German Research Foundation (DFG) for
489 funding (FOR 1598, ZE 533/9-1). The authors acknowledge support by Deutsche
490 Forschungsgemeinschaft and the Open Access Publishing Fund of Karlsruhe Institute of
491 Technology (KIT). The service charges for this open access publication have been covered by
492 a Research Centre of the Helmholtz Association. The code and the simulation projects
493 underlying this study are freely available on request.

494

495 **6 REFERENCES**

- 496 Beven, K., and Germann, P.: Macropores and water flow in soils revisited, *Water Resources*
497 *Research*, 49, 3071-3092, 10.1002/wrcr.20156, 2013.
- 498 Brooks, J. R., Barnard, H. R., Coulombe, R., and McDonnell, J. J.: Ecohydrologic separation
499 of water between trees and streams in a mediterranean climate, *Nature Geoscience*, 3, 100-
500 104, 10.1038/ngeo722, 2010.
- 501 Bronstert, A., Creutzfeldt, B., Graeff, T., Hajnsek, I., Heistermann, M., Itzerott, S., Jagdhuber,
502 T., Kneis, D., Lueck, E., Reusser, D., and Zehe, E.: Potentials and constraints of different
503 types of soil moisture observations for flood simulations in headwater catchments, *Natural*
504 *Hazards*, 60, 879-914, 10.1007/s11069-011-9874-9, 2012.
- 505 Davies, J., and Beven, K.: Comparison of a multiple interacting pathways model with a
506 classical kinematic wave subsurface flow solution, *Hydrological Sciences Journal-Journal*
507 *Des Sciences Hydrologiques*, 57, 203-216, 10.1080/02626667.2011.645476, 2012.
- 508 Delay, F., and Bodin, J.: Time domain random walk method to simulate transport by
509 advection-dispersion and matrix diffusion in fracture networks, *Geophysical Research*
510 *Letters*, 28, 4051-4054, 10.1029/2001gl013698, 2001.
- 511 Dentz, M., Gouze, P., Russian, A., Dweik, J., and Delay, F.: Diffusion and trapping in
512 heterogeneous media: An inhomogeneous continuous time random walk approach,
513 *Advances In Water Resources*, 49, 13-22, 10.1016/j.advwatres.2012.07.015, 2012.
- 514 Dingman, S. L.: *Physical hydrology*, McMillan, New York, 575 pp., 1994.
- 515 Elfeki, A. M. M., Uffink, G. J. M., and Lebreton, S.: Simulation of solute transport under
516 oscillating groundwater flow in homogeneous aquifers, *Journal of Hydraulic Research*, 45,
517 254-260, 2007.
- 518 Ewen, J.: 'Samp' model for water and solute movement in unsaturated porous media involving
519 thermodynamic subsystems and moving packets .2. Design and application, *Journal Of*
520 *Hydrology*, 182, 195-207, 10.1016/0022-1694(95)02926-5, 1996a.
- 521 Ewen, J.: 'Samp' model for water and solute movement in unsaturated porous media involving
522 thermodynamic subsystems and moving packets .1. Theory, *Journal Of Hydrology*, 182,
523 175-194, 10.1016/0022-1694(95)02925-7, 1996b.
- 524 Gayler, S., Woehling, T., Grzeschik, M., Ingwersen, J., Wizemann, H.-D., Warrach-Sagi, K.,
525 Hoegy, P., Attinger, S., Streck, T., and Wulfmeyer, V.: Incorporating dynamic root growth
526 enhances the performance of noah-mp at two contrasting winter wheat field sites, *Water*
527 *Resources Research*, 50, 1337-1356, 10.1002/2013wr014634, 2014.
- 528 Gerke, H. H., and Van Genuchten, M. T.: A dual-porosity model for simulating the
529 preferential movement of water and solutes in structured porous-media, *Water Resources*
530 *Research*, 29, 305-319, 1993.
- 531 Graeff, T., Zehe, E., Blume, T., Francke, T., and Schröder, B.: Predicting event response in a
532 nested catchment with generalized linear models and a distributed watershed model,
533 *Hydrological Processes*, n/a-n/a, 10.1002/hyp.8463, 2012.
- 534 Hassanizadeh, S. M., Celia, M. A., and Dahle, H. K.: Dynamic effect in the capillary
535 pressure-saturation relationship and its impacts on unsaturated flow, *Vadose Zone Journal*,
536 1, 38-57, 2002.
- 537 Holden, P. A. & N. Fierer (2005), *Microbial processes in the vadose zone*, *Vadose Zone J.*,
538 4(1), 1-21.
- 539 Jury, W., and Horton, R.: *Soil physics*, John Wiley, Cambridge, U.K., 2004.
- 540 Jury, W. A.: Simulation of solute transport using a transfer function model *Water Resources*
541 *Res.*, 18, 363 - 368, 1982



- 542 Kitanidis, P. K.: Particle-tracking equations for the solution of the advection-dispersion
543 equation with variable-coefficients, *Water Resources Research*, 30, 3225-3227,
544 10.1029/94wr01880, 1994.
- 545 Klaus, J., and Zehe, E.: Modelling rapid flow response of a tile drained field site using a 2d-
546 physically based model: Assessment of “equifinal” model setups, *Hydrological Processes*,
547 24, 1595 – 1609, DOI: 10.1002/hyp.7687., 2010.
- 548 Klaus, J., and Zehe, E.: A novel explicit approach to model bromide and pesticide transport in
549 connected soil structures, *Hydrology And Earth System Sciences*, 15, 2127-2144,
550 10.5194/hess-15-2127-2011, 2011.
- 551 Klaus, J., Zehe, E., Elsner, M., Kulls, C., and McDonnell, J. J.: Macropore flow of old water
552 revisited: Experimental insights from a tile-drained hillslope, *Hydrology And Earth System
553 Sciences*, 17, 103-118, 10.5194/hess-17-103-2013, 2013.
- 554 Klaus, J., Zehe, E., Elsner, M., Palm, J., Schneider, D., Schroeder, B., Steinbeiss, S., van
555 Schaik, L., and West, S.: Controls of event-based pesticide leaching in natural soils: A
556 systematic study based on replicated field scale irrigation experiments, *Journal Of
557 Hydrology*, 512, 528-539, 10.1016/j.jhydrol.2014.03.020, 2014.
- 558 Klaus, J., Chun, K. P., McGuire, K. J., and McDonnell, J. J.: Temporal dynamics of
559 catchment transit times from stable isotope data, *Water Resources Research*, 51, 4208-
560 4223, 10.1002/2014wr016247, 2015.
- 561 Kleidon, A., and Renner, M.: A simple explanation for the sensitivity of the hydrologic cycle
562 to surface temperature and solar radiation and its implications for global climate change,
563 *Earth System Dynamics*, 4, 455-465, 10.5194/esd-4-455-2013, 2013a.
- 564 Kleidon, A., and Renner, M.: Thermodynamic limits of hydrologic cycling within the earth
565 system: Concepts, estimates and implications, *Hydrology And Earth System Sciences*, 17,
566 2873-2892, 10.5194/hess-17-2873-2013, 2013b.
- 567 Koehler, B., Zehe, E., Corre, M. D., and Veldkamp, E.: An inverse analysis reveals
568 limitations of the soil-co₂ profile method to calculate co₂ production and efflux for well-
569 structured soils, *Biogeosciences*, 7, 2311-2325, 10.5194/bg-7-2311-2010, 2010.
- 570 Koehler, B., Corre, M. D., Steger, K., Well, R., Zehe, E., Sueta, J. P., and Veldkamp, E.: An
571 in-depth look into a tropical lowland forest soil: Nitrogen-addition effects on the contents
572 of n₂o, co₂ and ch₄ and n₂o isotopic signatures down to 2-m depth, *Biogeochemistry*, 111,
573 695-713, 10.1007/s10533-012-9711-6, 2012.
- 574 Loos, M., and Elsenbeer, H.: Topographic controls on overland flow generation in a forest -
575 an ensemble tree approach, *Journal Of Hydrology*, 409, 94-103,
576 10.1016/j.jhydrol.2011.08.002, 2011.
- 577 Martinez-Carreras, N., Udelhoven, T., Krein, A., Gallart, F., Iffly, J. F., Ziebel, J., Hoffmann,
578 L., Pfister, L., and Walling, D. E.: The use of sediment colour measured by diffuse
579 reflectance spectrometry to determine sediment sources: Application to the attert river
580 catchment (luxembourg), *Journal Of Hydrology*, 382, 49-63,
581 10.1016/j.jhydrol.2009.12.017, 2010.
- 582 Michalak, A. M., and Kitanidis, P. K.: Macroscopic behavior and random-walk particle
583 tracking of kinetically sorbing solutes, *Water Resources Research*, 36, 2133-2146,
584 10.1029/2000wr900109, 2000.
- 585 Mualem, Y.: A new model for predicting the hydraulic conductivity of unsaturated porous
586 media, *Water Resources Research*, 12, 513-522, 1976.
- 587 Neuweiler, I., Erdal, D., and Dentz, M.: A non-local richards equation to model unsaturated
588 flow in highly heterogeneous media under nonequilibrium pressure conditions, *Vadose
589 Zone Journal*, 11, 10.2136/vzj2011.0132, 2012.
- 590 Plate, E., and Zehe, E.: Hydrologie und stoffdynamik kleiner einzugsgebiete: Prozesse und
591 modelle, in, *Schweizerbart'sche Verlagsbuchhandlung (Nägele u. Obermiller)*, 366, 2008.



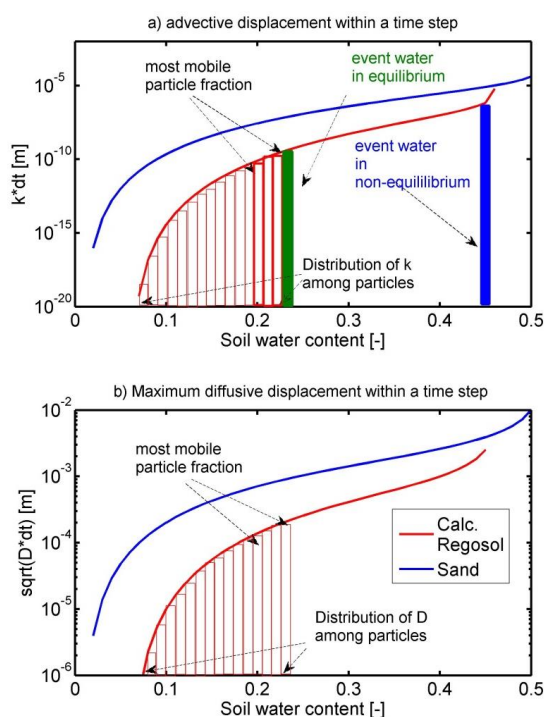
- 592 Roth, K., and Hammel, K.: Transport of conservative chemical through an unsaturated two-
593 dimensional miller-similar medium with steady state flow, *Water Resources Research*, 32,
594 1653-1663, 1996.
- 595 Saco, P. M., Willgoose, G. R., and Hancock, G. R.: Eco-geomorphology of banded vegetation
596 patterns in arid and semi-arid regions, *Hydrology And Earth System Sciences*, 11, 1717-
597 1730, 2007.
- 598 Šimůnek, J., Jarvis, N. J., van Genuchten, M. T., and Gärdenäs, A.: Review and comparison
599 of models for describing non-equilibrium and preferential flow and transport in the vadose
600 zone, *Journal of Hydrology*, 272, 14-35, 2003.
- 601 Tietjen, B., Jeltsch, F., Zehe, E., Classen, N., Groengroeft, A., Schiffers, K., and Oldeland, J.:
602 Effects of climate change on the coupled dynamics of water and vegetation in drylands,
603 *Ecohydrology*, 3, 226-237, 10.1002/eco.70, 2010.
- 604 Turner, D. D., Wulfmeyer, V., Berg, L. K., and Schween, J. H.: Water vapor turbulence
605 profiles in stationary continental convective mixed layers, *Journal Of Geophysical*
606 *Research-Atmospheres*, 119, 11151-11165, 10.1002/2014jd022202, 2014.
- 607 Uffink, G., Elfeki, A., Dekking, M., Bruining, J., and Kraaikamp, C.: Understanding the non-
608 gaussian nature of linear reactive solute transport in 1d and 2d, *Transport in Porous Media*,
609 91, 547-571, 10.1007/s11242-011-9859-x, 2012.
- 610 van Genuchten, M. T.: A closed-form equation for predicting the hydraulic conductivity of
611 unsaturated soils., *Soil Sci. Soc. Am. Jour.*, 44, 892 - 898, 1980.
- 612 van Schaik, N. L. M. B., Bronstert, A., de Jong, S. M., Jetten, V. G., van Dam, J. C., Ritsema,
613 C. J., and Schnabel, S.: Process-based modelling of a headwater catchment in a semi-arid
614 area: The influence of macropore flow, *Hydrological Processes*, 28, 5805-5816,
615 10.1002/hyp.10086, 2014.
- 616 Vogel, H. J., Cousin, I., Ippisch, O., and Bastian, P.: The dominant role of structure for solute
617 transport in soil: Experimental evidence and modelling of structure and transport in a field
618 experiment, *Hydrology And Earth System Sciences*, 10, 495-506, 2006.
- 619 Wienhoefer, J., and Zehe, E.: Predicting subsurface stormflow response of a forested hillslope
620 - the role of connected flow paths, *Hydrology And Earth System Sciences*, 18, 121-138,
621 10.5194/hess-18-121-2014, 2014.
- 622 Wrede, S., Fenicia, F., Martinez-Carreras, N., Juilleret, J., Hissler, C., Krein, A., Savenije, H.
623 H. G., Uhlenbrook, S., Kavetski, D., and Pfister, L.: Towards more systematic perceptual
624 model development: A case study using 3 luxembourgish catchments, *Hydrological*
625 *Processes*, 29, 2731-2750, 10.1002/hyp.10393, 2015.
- 626 Zehe, E., Elsenbeer, H., Lindenmaier, F., Schulz, K., and Bloschl, G.: Patterns of
627 predictability in hydrological threshold systems, *Water Resources Research*, 43, W07434
628 10.1029/2006wr005589, 2007.
- 629 Zehe, E., Blume, T., and Blöschl, G.: The principle of ‘maximum energy dissipation’: A
630 novel thermodynamic perspective on rapid water flow in connected soil structures, *Phil.*
631 *Trans. R. Soc. B*, 1–10, doi:10.1098/rstb.2009.0308, 2010a.
- 632 Zehe, E., Graeff, T., Morgner, M., Bauer, A., and Bronstert, A.: Plot and field scale soil
633 moisture dynamics and subsurface wetness control on runoff generation in a headwater in
634 the ore mountains, *Hydrology And Earth System Sciences*, 14, 873-889, 10.5194/hess-14-
635 873-2010, 2010b.
- 636 Zehe, E., Ehret, U., Blume, T., Kleidon, A., Scherer, U., and Westhoff, M.: A thermodynamic
637 approach to link self-organization, preferential flow and rainfall-runoff behaviour,
638 *Hydrology And Earth System Sciences*, 17, 4297-4322, 10.5194/hess-17-4297-2013, 2013.
- 639 Zehe, E., Ehret, U., Pfister, L., Blume, T., Schroeder, B., Westhoff, M., Jackisch, C.,
640 Schymanski, S. J., Weiler, M., Schulz, K., Allroggen, N., Tronicke, J., van Schaik, L.,
641 Dietrich, P., Scherer, U., Eccard, J., Wulfmeyer, V., and Kleidon, A.: Hess opinions: From



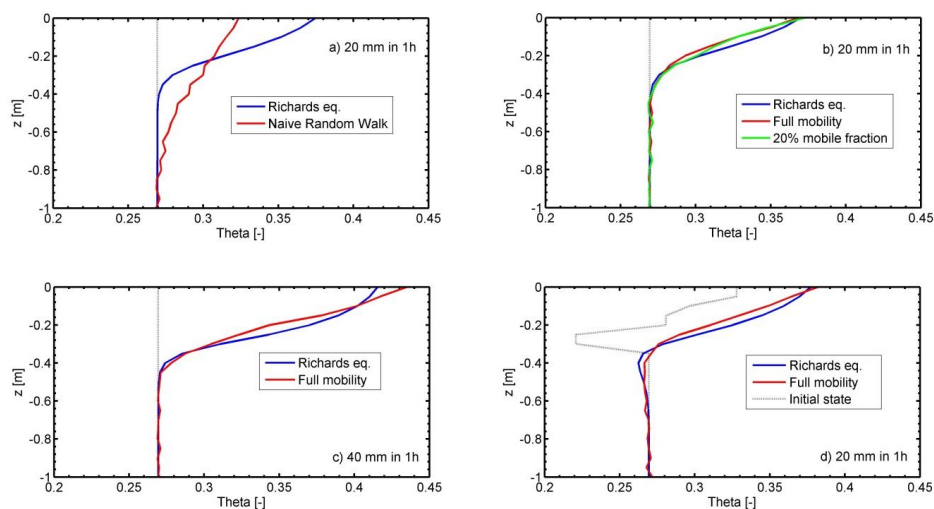
642 response units to functional units: A thermodynamic reinterpretation of the hru concept to
643 link spatial organization and functioning of intermediate scale catchments, Hydrology And
644 Earth System Sciences, 18, 4635-4655, 10.5194/hess-18-4635-2014, 2014.
645 Zimmermann, A., Schinn, D. S., Francke, T., Elsenbeer, H., and Zimmermann, B.:
646 Uncovering patterns of near-surface saturated hydraulic conductivity in an overland flow-
647 controlled landscape, Geoderma, 195, 1-11, 10.1016/j.geoderma.2012.11.002, 2013.
648



649 **7 FIGURES**



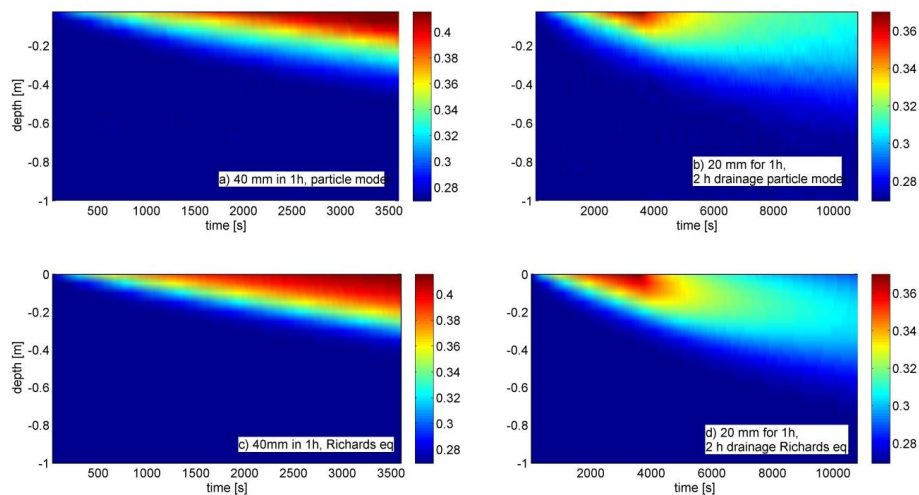
650
 651 Figure 1: Advective/drift displacement of a particle $k(\theta) dt$ (panel a) and maximum diffusive
 652 displacement $(D(\theta)dt)^{0.5}$ (panel b) plotted against soil water content for the sand on limestone
 653 in the Atert catchment and the Calcaric Regosol on loess in the Weiherbach catchment. The
 654 vertical bars visualize the distribution of the D among the particles, representing water in
 655 different pore size fractions. The arrows mark the most mobile particle fraction in the five
 656 upper soil moisture classes. The red and the blue rectangle highlight the case when treating
 657 event water either as in local equilibrium and particles travel according to $D((\theta(t+0.5\Delta t)))$ and
 658 $k((\theta(t+0.5\Delta t)))$ or when they enter the coarsest pores and travel according k_s .
 659



660

661 Figure 2: Final soil moisture profiles simulated for the sandy soil with the naive random walk
662 (panel a) and different versions of the particle model compared to the Richards equation for
663 two different block rains starting from the uniform initial state (panel c and b), and 20 mm
664 block rain on the s-shaped initial state (panel c). The dashed grey line marks the initial soil
665 moisture profiles.

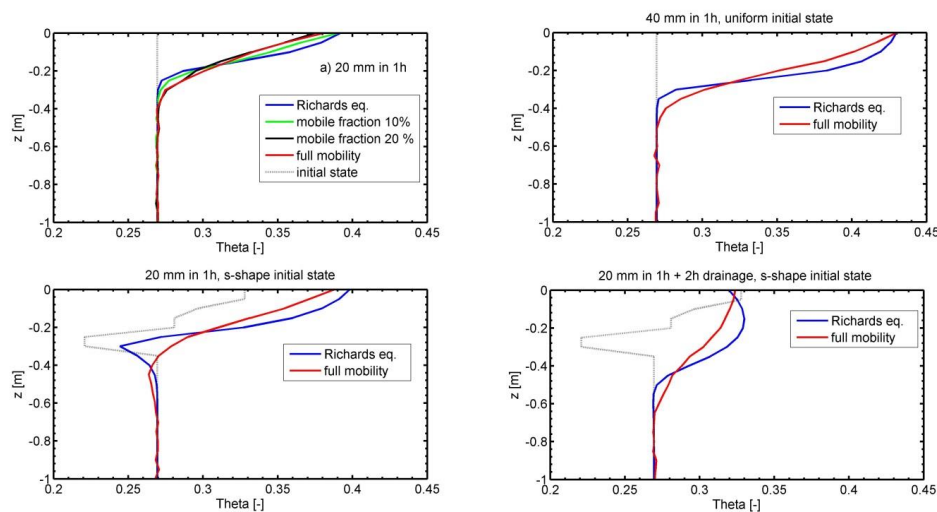
666



667

668 Figure 3: Time series of soil moisture simulated with the particle model and the Richards
669 solver for the sandy soil as 2d color plots for a simulated wetting event of 40 mm in 1 h (panel
670 a) particle model and c) Richards' solver) and a 1 h wetting and a 2 h drainage period (panel
671 b) particle model and d) Richards' solver).

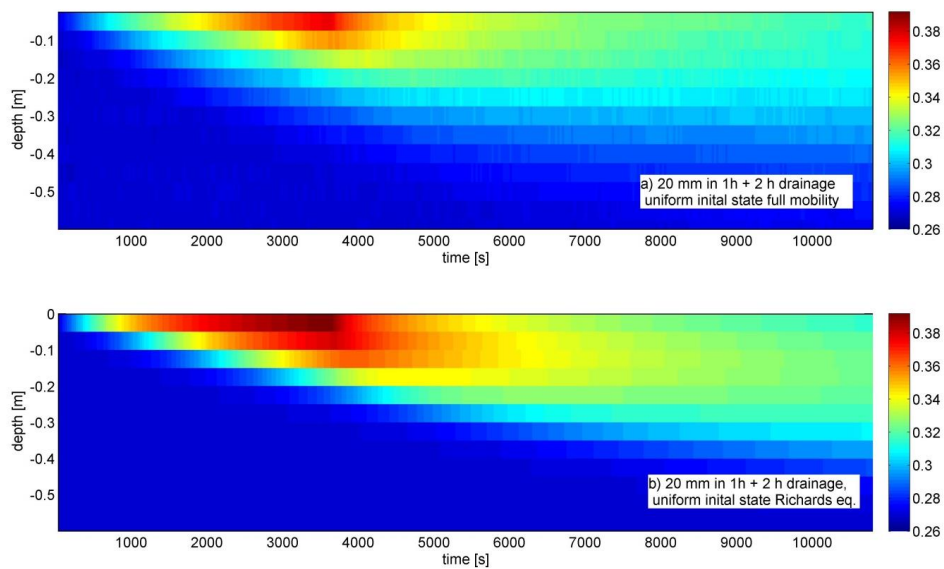
672



673

674 Figure 4: Final soil moisture profiles simulated for the young silty soil on schist. Panel a)
675 compares simulations with the full mobility particle model as well as versions assuming
676 mobile fractions of 10% or 20 %, respectively 20%. The remaining panels compare the full
677 class approach against the Richards equation starting from a uniform initial state after a 40
678 mm block rain (panel b), and from an s-shaped initial state after 20 mm of rainfall in 1 h
679 (panel c) and a subsequent drainage phase of 2h (panel d). The dashed grey line marks the
680 initial soil moisture profiles.

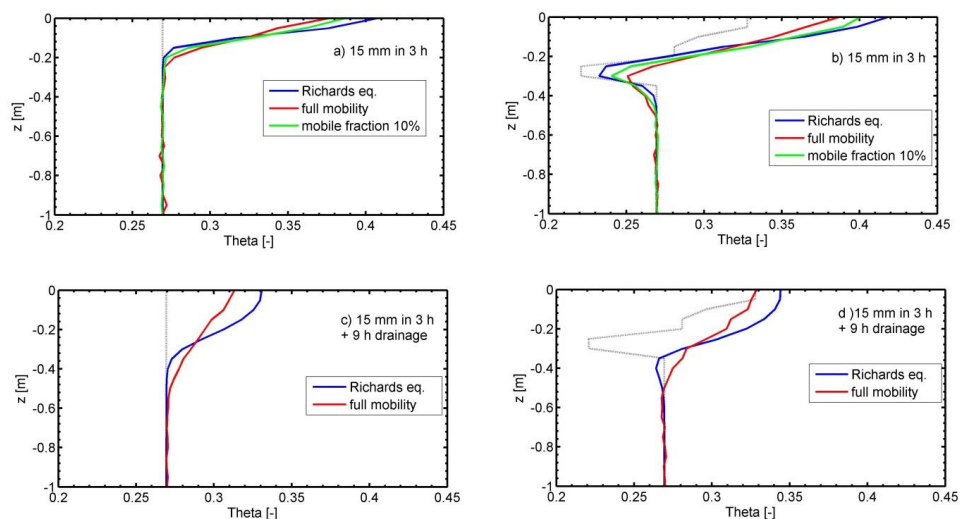
681



682

683 Figure 5: Time series simulated soil moisture profiles in the upper 60 cm: the full mobility
684 particle model in panel a) and the Richards solver in panel b) for the young silty soil on schist
685 for 20 mm infiltration of the uniform initial state and a subsequent drying of 2 hours.

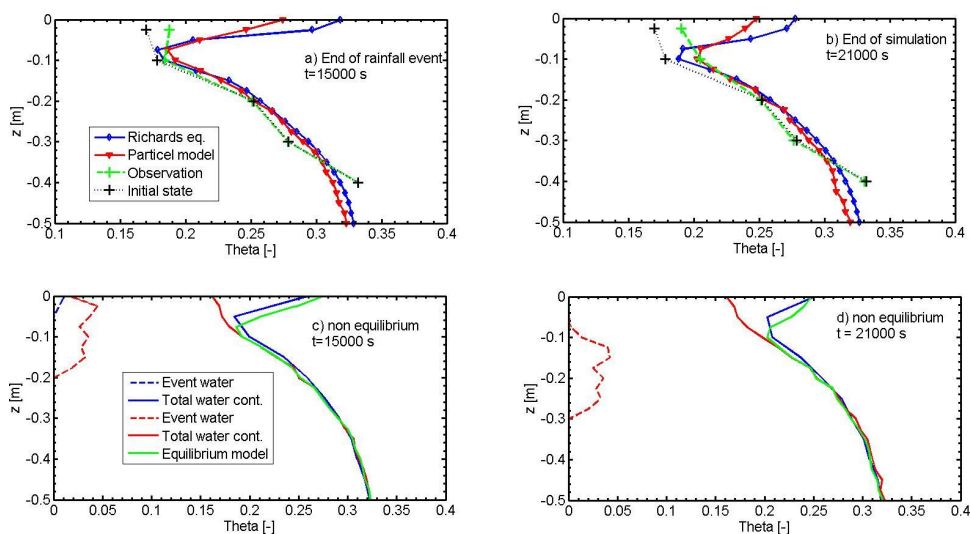
686



687

688 Figure 6: Final soil moisture profiles simulated for Calcaric Regosol on loess. Panels a) and b)
689 compare the particle model in the full mobility model (solid red) and in a mobile fraction of
690 10 % (solid green) to the Richards solver for 15 mm rainfall input in 3h. Panels c) and d)
691 compare the Richards solver and the particle model after 15 mm infiltration in 3 h and a
692 subsequent drainage phase of 9 h. The dashed grey line marks the initial soil moisture
693 profiles.

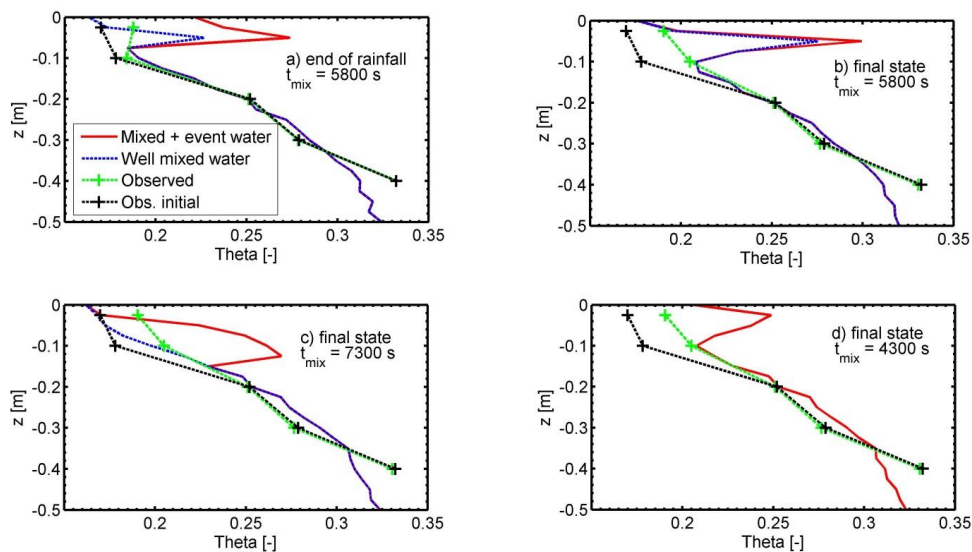
694



695

696 Figure 7: Soil moisture profiles simulated with the Richards equation (solid blue) and the
697 particle model (in the full mobility mode assuming equilibrium infiltration) compared to
698 observations in different depths at the end of the precipitation event (panel a), 15000s) and the
699 end of simulation (panel b), 21000s). Initial soil moisture observations are given as black,
700 intermediate and final observations as green crosses. Panels c) and d) present fractions of
701 event water (dashed lines) total water content (pre-event + mixed water) for simulations
702 assuming non-equilibrium infiltration. Blue lines correspond to $t_{\text{mix}} = 4300\text{s}$, red lines to $t_{\text{mix}} =$
703 7300s , the solid green line shows the soil water content simulated with equilibrium
704 infiltration.

705



706

707 Figure 8: Non equilibrium simulations compared against observed soil moisture values, for
708 $t_{\text{mix}} = 5800\text{s}$ after the rainfall event (panel a) and at the end of simulation (panel b). Panel c)
709 and d) present the final state for $t_{\text{mix}} = 7300\text{s}$ or $t_{\text{mix}} = 4300\text{s}$, respectively.

710

711 **8 TABLES**

712

713 Table 1: Soil hydraulic parameters of the sandy soil on limestone, the young silty soil on
 714 schist and the Calcaric Regosol on loess: saturated hydraulic conductivity k_s , saturated and
 715 residual water contents θ_s , θ_r , air entry value α , shape parameter n .

Soil type	k_s [m/s]	θ_s [-]	θ_r [-]	α [m ⁻¹]	n [-]
Sand on limestone	$2.23 \cdot 10^{-4}$	0.508	0.01	4.71	1.475
Young silty soil on schist	$2.62 \cdot 10^{-4}$	0.51	0.12	6.45	1.50
Calc. Regosol on loess	$6.0 \cdot 10^{-6}$	0.46	0.06	1.50	1.36

716

717



718

719 Table 2: Characteristics of the numerical benchmarks: rainfall input P, initial condition θ_{ini} ,720 simulation time t_{sim}

Soil type	Wetting	Wetting	Wetting	Wetting & drying
Sand	P =20 mm in 1h θ_{ini} = uniform t_{sim} =1h	P =40 mm in 1h θ_{ini} = uniform t_{sim} =1h	P =20 mm in 1h θ_{ini} = s-shape t_{sim} =1h	P =20 mm in 1h θ_{ini} = uniform t_{sim} =3h
Silty soil	P =20 mm in 1h θ_{ini} = uniform t_{sim} =1h	P =40 mm in 1h θ_{ini} = uniform t_{sim} =1h	P =20 mm in 1h θ_{ini} = s-shape t_{sim} =1h	Input: 20 mm in 1h initial con.: uniform Duration: 2h
Calc. Regosol	P =20 mm in 1h θ_{ini} = s-shape t_{sim} =1h	P =20 mm in 4h θ_{ini} = uniform t_{sim} =4h	P =15 mm in 3h θ_{ini} = s-shape t_{sim} =3h	P =15 mm in 3h θ_{ini} = uniform t_{sim} =6h

721

722



723 Table 3: Top soil and the subsoil hydraulic properties at the central meteorological station in
724 the Weiherbach catchment: saturated hydraulic conductivity k_s , saturated and residual water
725 contents θ_s , θ_r , air entry value α , shape parameter n .

Depth [m]	k_s [m/s]	θ_s [-]	θ_r [-]	α [m ⁻¹]	n [-]
0 - 0.3	$6.0 \cdot 10^{-6}$	0.46	0.06	1.50	1.36
> 0.3	$3.4 \cdot 10^{-6}$	0.44	0.06	1.50	1.36

726

727

728

729